



Effect of displacement rates on the mechanical integrity of soft-porous rock analogue containing non-persistent joints of variable lengths

GAURAV KUMAR MATHUR¹, VIKRAM MAJI¹, SANTANU MISRA^{1,*}  and GAURAV TIWARI²

¹Experimental Rock Deformation Laboratory, Department of Earth Sciences, Indian Institute of Technology Kanpur, Kanpur, Uttar Pradesh 208 016, India.

²Department of Civil Engineering, Indian Institute of Technology Kanpur, Kanpur, Uttar Pradesh 208 016, India.

*Corresponding author. e-mail: smisra@iitk.ac.in

MS received 11 June 2021; revised 5 January 2022; accepted 7 January 2022

We investigated the effects of displacement rates on the strength and mechanisms of fracturing by conducting three series of compressive experiments with synthetic samples analogous to soft-porous rocks. The three series correspond to (i) intact samples (without joints), (ii) samples with single joint of different lengths (10, 15, 20 and 25 mm) and (iii) samples with double joint-segments (15 mm each separated by a bridge), respectively. The samples were deformed under variable displacement rates (0.048, 0.12, 3, 4.45 and 6 mm/min). We found that the material-strength enhanced with increasing displacement rates for intact and samples with single joint-segment with limited persistent ratio; however, the strength declined substantially for samples with persistent ratio above a threshold (~ 0.20) and beyond a critical window of displacement rates (3–4.45 mm/min) for both the samples with single- and double-joint-segment(s). The fractures were dominated by tensile wing cracks, however, the location, timing and corresponding displacement rates concerning the appearance of secondary shearing confirmed that the extent of shearing mechanism enhanced at fast-displacement rates when the persistent ratio crossed a critical value (~ 0.20). Overall, the strength of material considerably reduced and the potential of damage further accelerate at faster displacement rates when the persistent ratio of non-persistent joint(s) crossed a pedantic threshold.

Keywords. Analogue-experiments; persistence ratio; strength of rocks; tensile wing crack.

1. Introduction

Rocks in natural conditions mostly contain discontinuities in a wide range of scales, from micro-cracks to joints and regional faults. Some of them are continuous (persistent), while most are non-persistent. The presence of discontinuities significantly influences the mechanical properties of the rock mass (Miller and Deere 1966; Lajtai 1971; Hoek and Bray 1974; Misra 2011) as they act as

zones of high-stress concentration favouring initiation or reactivation of cracks (Griffith 1921; Eshelby 1959; Rudnicki and Rice 1975; Mandal *et al.* 2004; Misra and Mandal 2007; Misra *et al.* 2009, 2015) and foster decrease in strength. Weakening of rock mass enhances the risk of different stress-induced (e.g., thermal, seismic, blast loading, overburden, etc.) and structurally controlled failures (Wyllie and Mah 2004), that are mostly reported from construction sites such as for

tunnels, natural and man-made slopes, foundations, and underground excavations. Earlier works investigated the effect of different attributes of discontinuities that enhance the risk of failure such as roughness (Atapour and Moosavi 2014), orientation (Bobet and Einstein 1998), joint matching (Zhao 1997), frequency (Sagong and Bobet 2002; Horii and Nemat-Nasser 1986). However, there is dearth of information on the consequences of joint persistence, i.e., the areal extent to which joints are retained before terminating into surrounding material or against other discontinuities (Mauldon 1994), on rock failure. This is also evident in standard rock mass classification schemes, such as Q-system (Barton *et al.* 1974) and Geological Strength Index (Hoek and Brown 1997). Also, the presence of joints with variable persistence ratios, defined as the ratio of the sum of trace lengths of all joint-segments to the length of collinear line connecting the joint-segments (Dershowitz and Einstein 1988), related to the analysis of slope and tunnel instability have not received much attention. This could lead to significant inaccuracies in the estimation of strength, deformation, and failure behaviour of rocks intersected with non-persistent joints, as reported in recent investigations (Xu *et al.* 2013; Alshkane *et al.* 2017; Vazaios *et al.* 2018; Shaunik and Singh 2019).

Another important concern is the displacement rate or strain rate that consequentially influences the estimation of material strength (Lankford 1981; Olsson 1991). It has been established that brittle materials respond in three different ways as functions of displacement rates: (i) creep of the bulk material between cracked surfaces, (ii) strain rate dependency of the growing microcracks, and (iii) influence of inertial forces of the material (Ožbolt *et al.* 2006). In practice, a combination of these three effects interplays, depending on the displacement rate and the type of material used. For quasi-brittle materials, like concrete, creeping between the fracture surfaces mostly controls the damage mechanisms at slow-displacement rates, while the other two effects dominate during fast-displacement rates. Earlier studies reported that the strength of material enhances rapidly when strain rates exceeded a critical value (Kumar 1968; Perkins *et al.* 1970) and the observation was attributed to the inertial confinement (Janach 1976). Several recent investigations (Jafari *et al.* 2004; Tiwari and Latha 2019) noted changes in the mechanical behaviour of material at varying displacement rates, however, the dynamics are poorly

understood as most of the studies correspond to pseudo-static displacement rates. In practical situations, such as blasting, drilling, thermal and seismic forces often lead to dynamic displacement conditions (Atapour and Moosavi 2014) and demand the need for detailed investigations on material strength anisotropy at varying rates of displacement. It is difficult to reproduce the true dynamic natural conditions in the laboratory due to technical and logistical constraints, but the outcome from the static uniaxial compression tests with a wide range of displacement rates can be projected to predict the consequences in natural situations with consideration of the boundary conditions.

The present research integrates the influence of variable displacement rates on molded gypsum samples intersected with non-persistent joint-segment(s) of different dimensions and their corresponding fracture patterns. The samples are analogous to soft-porous rocks, like semi-lithified sediments, sedimentary rocks with poor cohesive strength and weathered rocks. In this study, we have tested two novel hypotheses. The first hypothesis evaluated displacement enhancement of the strength of intact material, and material containing single- and double-jointed segments at fast-displacement rates. The potential of initiating and expanding shear movement with increasing displacement rates has been assessed in the second hypothesis. The hypotheses were tested by carrying out three series of experiments on cylindrical samples containing artificial joint(s) at varying displacement rates. The displacement rate dependency of samples containing joint(s) was then compared with the corresponding responses of intact samples.

2. Experimental methods

2.1 Sample preparation

Experimental investigations on jointed rocks are split into two main groups. The first group used rocks containing natural joints or fabricated artificial joint-segments using a saw machine or hydraulic press (Barton 1973; Kronenberg *et al.* 1990; Ishii 2016). The second group used samples made of artificial materials, such as cement, gypsum, polymethylmethacrylate (PMAA), polycarbonate (PC), etc. (Lajtai 1971; Horii and Nemat-Nasser 1986; Kulatilake *et al.* 1997; Sagong and

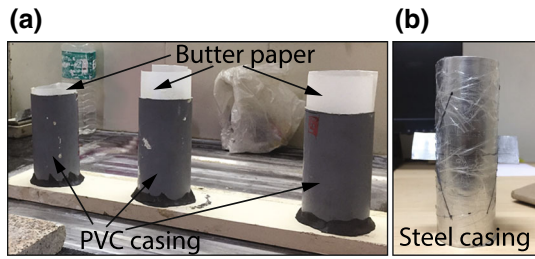


Figure 1. (a) Intact and (b) jointed mold used for sample preparation. Intact samples were prepared inside a PVC pipe. The samples with simulated joint(s) are prepared inside steel canisters with predefined slits.

Bobet 2002; Misra *et al.* 2009, 2015; Sun *et al.* 2014; Wasantha *et al.* 2014). Each method of selection of specimens has its advantages and disadvantages, however, working with natural samples manifested inherent variability which restrict to isolate the effect of the governing parameters of interest. To avoid such constraints, analogue samples made of gypsum have been used in the present experiment following the second group. Additionally, mechanical properties of gypsum-like rock materials have been well characterized under different experimental conditions (Wei *et al.* 2020).

The samples were prepared by mixing Plaster of Paris ($\text{CaSO}_4, 1/2\text{H}_2\text{O}$) with water in 0.6:1 ratio by weight to form gypsum ($\text{CaSO}_4, 2\text{H}_2\text{O}$) and the mixture was then transferred into a cylindrical PVC mold (figure 1a) for producing cylindrical samples with 50 mm in diameter and 100 mm in height, after post-processing, i.e., grinding the end surfaces. These samples were dried for ~ 10 days at room temperature to achieve sufficient cohesion. Mixing of the ingredients, casting, and curing processes for the preparation of samples were carefully maintained to ensure reproducibility.

Three different sets of samples were prepared: (i) intact samples, i.e., samples without any joint-segment (figure 2a), (ii) samples with single joint-segment at identical inclination with respect to the displacement axis but different in lengths (figure 2b–e), and (iii) samples with two joint-segments (figure 2f). A thin planar aluminum slit of 0.16 mm in thickness was used to prepare the single joint-segmented samples of different lengths, i.e., 10, 15, 20, and 25 mm corresponding to persistence ratios of 0.10, 0.15, 0.20 and 0.25, respectively (figure 1b). Two identical aluminum slits with 15 mm width were used for preparing jointed samples of double segments (0.30 persistence ratio) with an intact intermediate bridge of similar length. In all samples, the slit was positioned at 30° inclination

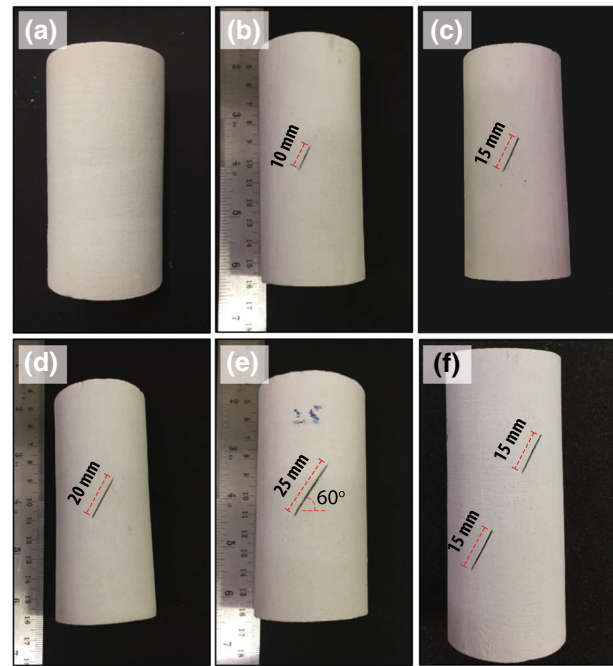


Figure 2. Photographs of the representative samples used in the experiments. (a) Intact samples (i.e., sample without any joint), (b–e) samples with single joint of 10, 15, 20 and 25 mm lengths, respectively, and (f) sample with two joints of 15 mm length. All samples are $100 (\pm 3)$ mm in length and $50 (\pm 2)$ mm in diameter.

with the cylinder axis. The specific value of the dip angle was considered as the axial stress required for sliding along the joint or pre-existing flaw is minimum when the tilting is at 30° with the maximum compressive stress direction (Lajtai 1971; Ramamurthy and Arora 1994; Ghazvinian and Hadei 2012; Sun *et al.* 2014). Also, the development of compression-induced wing cracks started at the crack tip when the inclination of pre-existing flaw positioned at 30° with respect to the maximum compression direction and any deviation from this value would result in shifting the initiation location of newly formed wing cracks from crack tip. We cannot discount the possibility that varying angle of inclination of the inherent flaw influences the coefficient of friction hence the identical value of inclination was maintained throughout the experiments to limit the specimen geometry-induced heterogeneity.

2.2 Experimental procedure

Before conducting the destructive tests, the average interconnected porosity (48%) of the intact samples was estimated using an automated gas pycnometer. The compression tests were carried

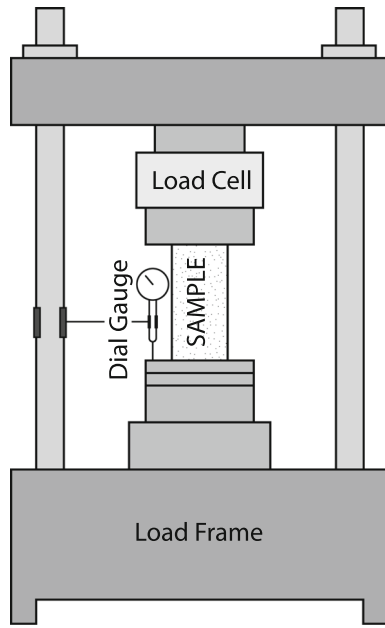


Figure 3. Schematic illustration of the uniaxial deformation apparatus used in this study.

out using a uniaxial testing machine operated under displacement-controlled mode (mm/min) with a maximum capacity of 50 kN (figure 3). The load frame performs under a range of desired displacement rates (0.048–6 mm/min, in our case) and is controlled by a motor drive system. A dial gauge (resolution 0.01 mm, accuracy $\pm 12 \mu\text{m}$) attached to the displacement frame was used for measuring axial displacements and converted later to compressive strains.

3. Results

3.1 Deformation of intact samples

The stress–strain responses and the failure strengths of the intact gypsum samples at five different displacement rates are presented in figure 4 and the results are summarized in table 1. The lowest (3.62 MPa) and highest (5.47 MPa) strength were observed when the axial displacement rate was minimum (0.048 mm/min) and maximum (6 mm/min) accordingly. In case of very slow to medium displacement rates, samples experienced plastic deformation, i.e., deformation phase between yield and final brittle fracturing, until the failure strengths were reached. Samples deformed under fast to very fast rates broken down immediately after yield without any notion of plasticity. Overall, there was a gradual increase in

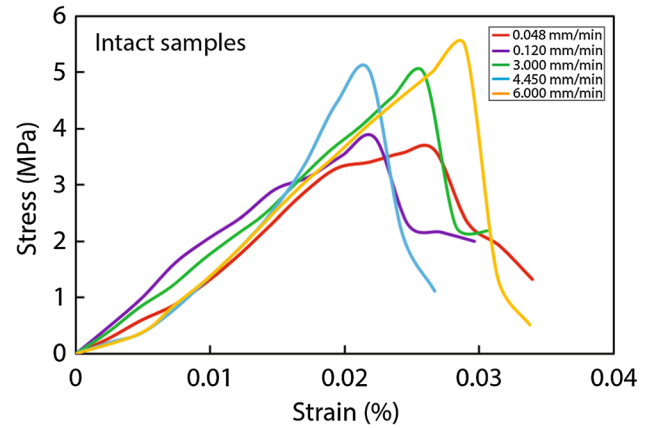


Figure 4. (a) Stress–strain curve of intact samples at different displacement rates. At displacement rate of 6 mm/min, the failure strength is highest, while lowest observed at 0.048 mm/min rate.

failure strength as the rate of displacement enhanced for the intact samples.

Samples mostly failed under tensile split mode and caused bifurcation of materials on either side along the fracture surfaces. At very slow rate of displacement (0.048 mm/min), crack developed at the top bounding face of the sample and started to propagate downwards along the central compression axis (figure 5a) while slow (0.12 mm/min) to fast (4.45 mm/min) rates initiated cracks near the base followed by upward movement as the displacement rate increases (figure 5b–d). At very fast rate of displacement (6 mm/min), the intact sample mostly broke apart (figure 5e) with small-sized fragments ejected in the test chamber at high speed. This is also evident in the stress–strain curve marked by sharp decline (figure 4a, yellow line) when the strength reached peak. Overall, the intact samples mostly failed under tensile splitting modes and sometimes developed multiple cracks, propagated in the top-down and bottom-up directions along the central loading axis.

3.2 Deformation of samples containing single joint-segment

The molded cylindrical gypsum casts with single fabricated joint-segment of variable lengths (total 20 samples) representing non-persistent joint within an artificial rock mass, were compressed uniaxially at different displacement rates (from very slow to very fast), and the failure mechanisms of different samples are shown in figure 6. The stress–strain responses of samples with the corresponding lengths of joint-segment are displayed in

Table 1. Failure strength (in MPa) and maximum change (in %) of the strengths of the intact (series one), single (series two) and double (series three) jointed samples at different displacement rates.

| Length of segment | Displacement rates (mm/min) | | | | | Mean | Overall % change |
|-------------------|-----------------------------|-------------|------------|-------------|---------------|-------------|------------------|
| | 0.048 (very slow) | 0.12 (slow) | 3 (medium) | 4.45 (fast) | 6 (very fast) | | |
| Intact | 3.62 | 3.84 | 4.98 | 5.08 | 5.47 | 4.6 ± 0.82 | 51.10 |
| 10 mm | 2.81 | 2.73 | 3.07 | 3.29 | 4.4 | 3.26 ± 0.67 | 56.58 |
| 15 mm | 3.51 | 3.79 | 3.5 | 3.59 | 3.94 | 3.67 ± 0.19 | 12.25 |
| 20 mm | 2.83 | 2.87 | 3.45 | 2.36 | 2.21 | 2.74 ± 0.49 | -21.91 |
| 25 mm | 2.4 | 2.83 | 2.91 | 2.13 | 2.04 | 2.46 ± 0.39 | -15.00 |
| Double | 2.86 | 2.2 | 2.52 | 2.33 | 2.08 | 2.40 ± 0.31 | -27.27 |

Note: Unit of strength is in MPa.

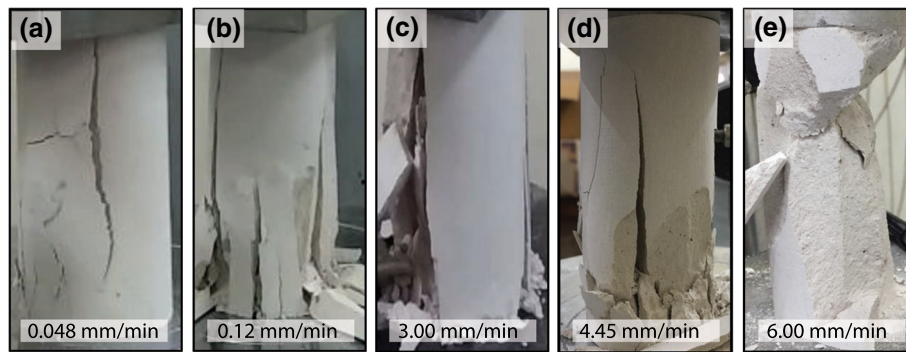


Figure 5. Photographs of the intact samples after failure and tested at various displacement rates (a) 0.048 mm/min, (b) 0.12 mm/min, (c) 3 mm/min, (d) 4.45 mm/min, and (e) 6 mm/min.

figure 7. Table 1 summarized the experimental results for samples containing single joint-segment and is discussed in detail in the following subsections.

3.2.1 Samples with 10 mm length of joint-segment

A progressive increase in failure strength was recorded with the increment in displacement rates (figure 7a), however, the failure strength at very slow displacement rate (2.81 MPa at 0.048 mm/min) exceeded than that of the slow rate (2.73 MPa at 0.12 mm/min) (red and violet curves in figure 7a). The samples compressed under very fast (6 mm/min) and medium (3 mm/min) displacement rates experienced sharp stress decline (yellow and green curves in figure 7a) while a post-yield plastic deformation, as evidenced from gradual stress drop till the attainment of failure strength, for the rest of the displacement rates. The failure strength of the samples with 10 mm joint-segment was comparatively lower than that of the intact

samples at their equivalent rate of displacement. Also, the peak failure strain accumulation (0.03) occurred when the rate was very fast similar to the intact samples.

The patterns of failure for samples with 10 mm joint-segment varies with the rate of displacement (figure 6a–e). At very slow (0.048 mm/min) to slow (0.12 mm/min) displacement rates, development of wing cracks was observed at the tips of the non-persistent joint-segments. Medium (3 mm/min) to very fast (6 mm/min) rates of displacement caused rapid failure of the samples. In addition to the wing cracks, several shear cracks propagating from the bounding faces towards the center of the samples and merging with the wing cracks were developed when the displacement rates were medium (3 mm/min) and fast (4.45 mm/min). Fast to moderate rates allowed simultaneous growth of both wing and compression induced cracks causing the material to fail under tensile-shear mixed mode. Overall, tensile wing cracks were predominant throughout all the ranges of the displacement rates, however, shearing mode also observed when

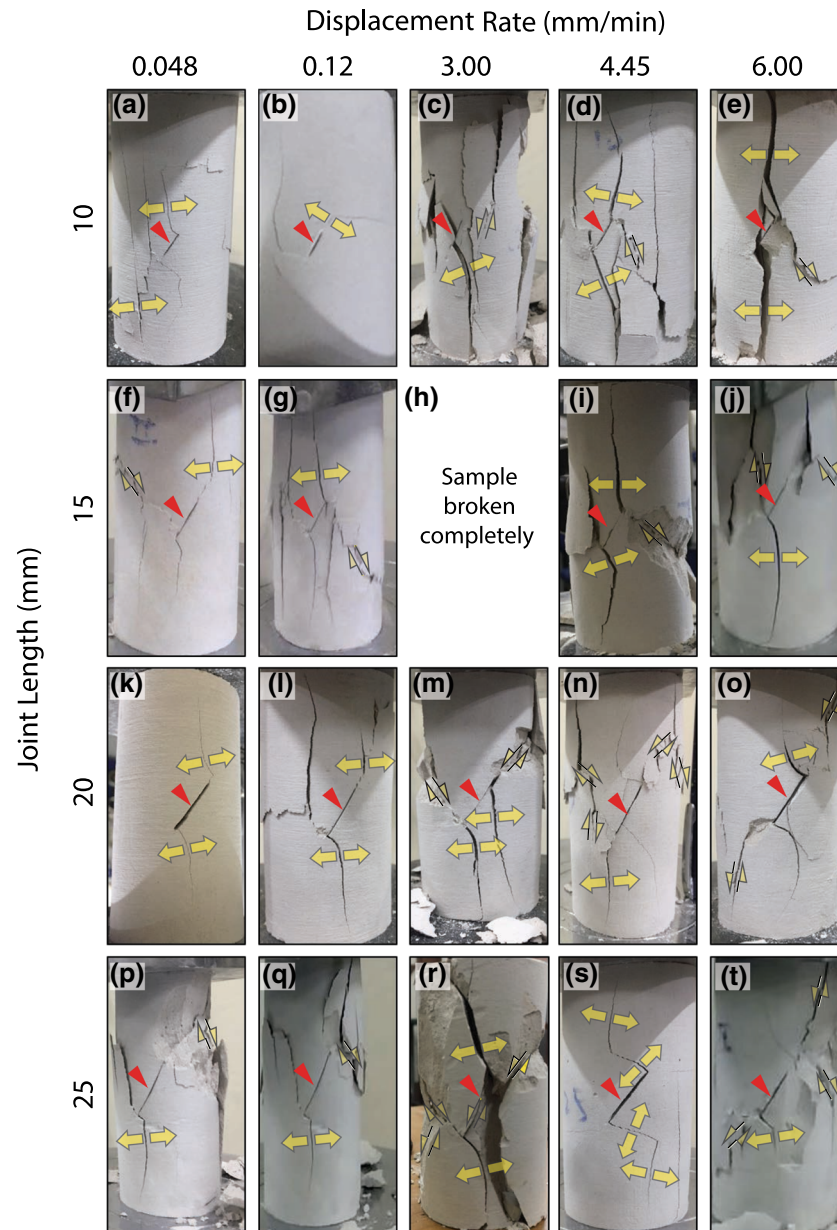


Figure 6. Mechanisms of crack propagation and coalescence at different displacement rates for samples with variable lengths of single joint-segment (a–e) 10 mm, (f–j) 15 mm, (k–o) 20 mm, and (p–t) 25 mm. Red arrowhead mark the locations of induced joint-segment; tensile wing cracks and shear cracks were represented by yellow arrows with the arrowhead specifying the directions of fracture movement.

the rate crossed a threshold of 3 mm/min (medium).

3.2.2 Samples with 15 mm length of joint-segment

Different rates of axial displacement mostly caused plastic deformation of samples except at very slow and very fast (red and yellow curves in figure 7b at 0.048 and 6.0 mm/min) rates. Peak failure strain accumulation (0.03%) occurred at medium displacement rate. However, the maximum strength

was recorded at very fast displacement rate. Overall, the enhancement of displacement rates increases strength of material, however, the increment was sometimes interrupted with instant decrease in strength as observed at medium rate of displacement (green curve in figure 7b at 3 mm/min).

The types of cracking patterns vary with the rate of displacement as shown in figure 6(f–j). Tensile wing crack developed and propagated slowly towards the bounding surfaces of the samples. Secondary shearing was observed later with the

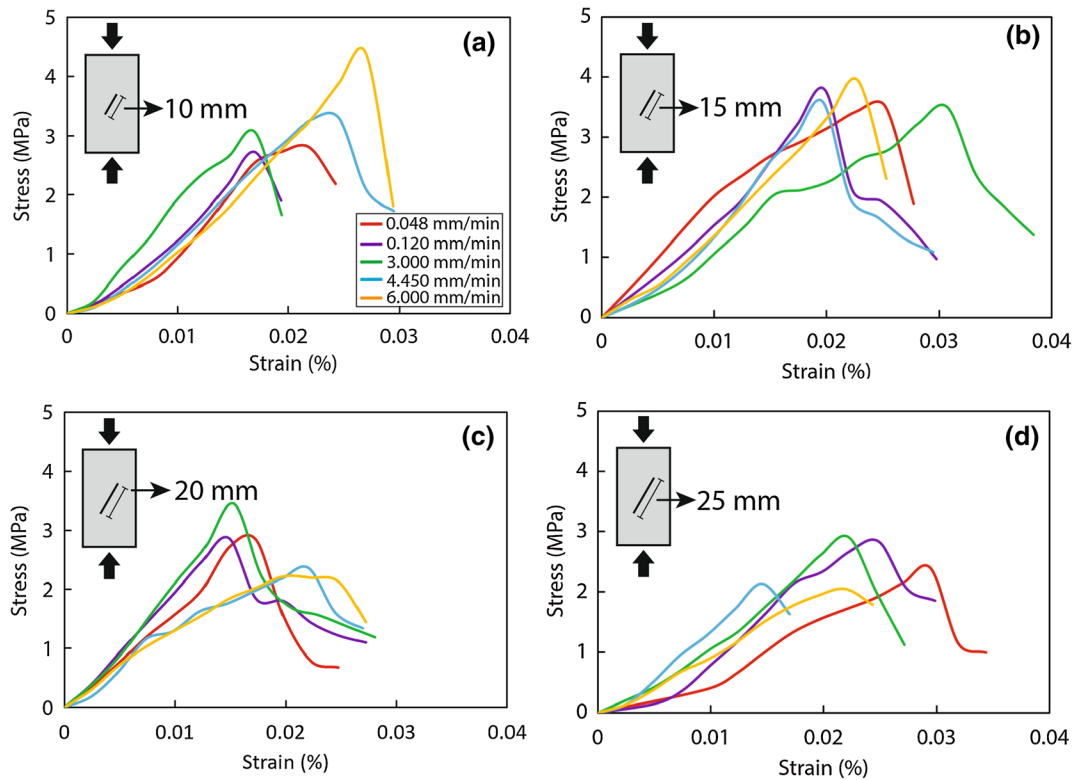


Figure 7. Stress–strain curves of the samples with a single joint-segment of variable lengths and tested under a range of displacement rates. The legend in (a) applies to (b), (c), and (d).

increasing length of the wing cracks at different rates of axial displacement except for medium rate (3 mm/min). Release of maximum failure strain (0.03%) accumulated during moderate rate of displacement broke the sample apart and material fragments were ejected at random directions (green curve in figure 7b). Overall, tensile wing cracks developed at the crack tips initiated secondary shearing when the fracture reached an optimum length.

3.2.3 Samples with 20 mm length of joint-segment

The mean magnitude of the failure strength substantially reduced for samples with 20 mm (2.74 ± 0.49 MPa) jointed segments compressed under different displacement rates than compared to 10 mm (3.26 ± 0.67 MPa) and 15 mm (3.67 ± 0.19 MPa) jointed segments (figure 7c). Accumulation of peak failure strain ($\sim 0.02\%$) occurred at fast to very fast-displacement rates. A progressive increase in failure strength was observed from very slow to medium rates of displacement followed by substantial decline as the rates continue to increase from fast to very fast.

The samples underwent brittle failure at relatively low stress by developing quasi-coplanar secondary shear cracks along the direction of initial joint-segment in addition to the wing cracks (figure 6k–o). The secondary cracks were noticed for all the displacement rates except at 0.48 mm/min rate. Overall, the development of quasi-coplanar secondary shear cracks was observed along the direction of the induced joint-segment with relatively high persistent ratio in addition to the tensile wing cracks. Also, faster displacement rates enhance the probability of forming shear fractures over the slow rates.

3.2.4 Samples with 25 mm length of joint-segment

The stress–strain relationships for samples with 25 mm joint-segment reveal (figure 7d) that the material experienced varying degrees of post-yield plastic deformation at different displacement rates except at 6 mm/min rate. Peak failure strain ($\sim 0.03\%$) accumulated when the rate of displacement was very slow, which is contrastingly different than the rest of the structural configurations of specimens. Substantial reduction in mean failure

strength (2.42 ± 40 MPa) was recorded when compared with samples having 10 mm (3.26 ± 0.67 MPa) and 15 mm (3.67 ± 0.19 MPa) joint-segment. However, mean failure strength was comparable with samples containing 20 mm (2.74 ± 0.49 MPa) joint-segment. The strength of the material registered an initial progressive increase with the increment in the displacement rate and reached maximum strength (2.91 MPa) at medium (3 mm/min) displacement rate. Following the peak, there was progressive reduction in strength with increasing displacement rate. A nonlinear change in stress–strain relationship was noticed when the rate of displacement crossed a threshold of 3 mm/min (medium rate).

The samples were substantially broken down at relatively low stress window when the persistent ratio of the single joint-segment was highest, and material failed under secondary shear movements followed by the primary tensile cracks (figure 6p–t). At very slow and slow displacement rates, early development of quasi-coplanar secondary shear crack initiated failure along the induced fractured surfaces which are in contrast with smaller persistent ratios. Extensive damage occurred at medium rate, while fast and very fast rates allowed the development of prominent tensile wing cracks with occasional shearing. Overall, the increase in joint persistent ratio caused early development of quasi-coplanar secondary shear fracture and slow rate gradually caused creep of the bulk material along the induced cracked surfaces.

3.3 Deformation of samples containing two joint-segments

An overall decrease in mean failure strengths (2.40 ± 0.31 MPa) was recorded than single jointed samples (figure 8). A sharp stress drop following attainment of failure strength at very fast to medium displacement rates and a progressive stress drop after peak failure strength at slow to very slow displacement rates was observed. Overall, the strength of the samples progressively increased with increasing displacement rates ranging from very slow to medium. With further increment in displacement rates from fast to very fast, the strength contrastingly decreased. Peak failure strain accumulated (0.02%) at very fast displacement rate (6 mm/min), while maximum failure strength recorded at medium rate (3 mm/min).

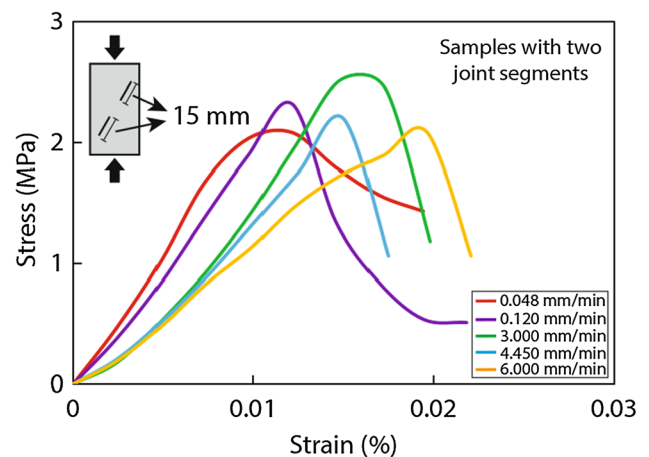


Figure 8. Stress–strain curve of the samples with two joint-segments and tested at varying displacement rates.

Most of the samples display primary wing cracks around the tips of the joint-segments positioned in the upper and lower half of the sample (figure 9). Shearing mode was absent at slow rates even with highest persistent ratio (overall 30 mm) but with a bridge in between the induced joint-segments unlike samples with 25 mm joint-segment that had developed early shear fracture. At medium- to fast-displacement rates, quasi-coplanar secondary shear fracture developed in the bridge area connecting the separated joint-segments. Very fast-displacement rate, on the other hand, initiate faint secondary shear crack due to limited time span. Overall, we observed that the development of shear crack was limited at slow rates when the induced joint-segments were separated by a bridge, but faster rates allow the formation of quasi-coplanar secondary shear fracture mostly within the bridging region connecting the weakly developed primary tensile wing cracks.

4. Discussion

4.1 Dependency of displacement rates on strength of material

The effect of displacement rate dependency on the strength and mechanical behaviour of molded gypsum cast representing artificially jointed rock was examined in this study. The first hypothesis testing the fact that strength of material enhances with increasing displacement rate holds true for the intact samples and samples with low persistent ratio (0.10 and 0.15), however, partially true for samples with high persistent ratios (0.20 and 0.25) up to a critical value (3 mm/min in our

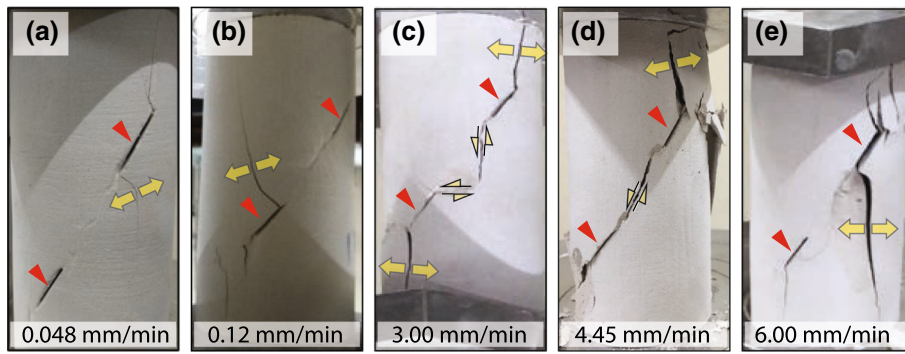


Figure 9. Fracture pattern of samples with two joint-segments of 15 mm length separated by a bridge of identical length and tested at different displacement rates (a) 0.048 mm/min, (b) 0.12 mm/min, (c) 3 mm/min, (d) 4.45 mm/min, and (e) 6 mm/min.

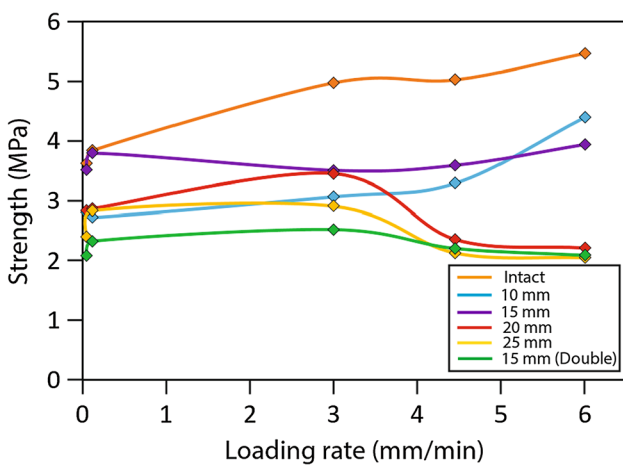


Figure 10. Failure strengths of the samples from three series of experiments (intact, single and double jointed) at different displacement rates.

investigation) of the displacement rate beyond which material strength decreases (figure 10). The increment in strength under experimental displacement rates for intact samples and samples with 10 and 15 mm joint-segments are 51.10, 56.58 and 12.25%, respectively, while the overall strength reduction of samples with 20 and 25 mm joint-segments are 21.91, 15 and 27.27%, respectively (table 1). Tiwari and Latha (2019) estimated 18.37% reduction in strength of the jointed rock samples intersected with persistent joints at slow to fast (0.05–15 mm/min) displacement rates which is partially in agreement with our observation for non-persistent joint-segments with longer lengths. In addition, Gong *et al.* (2019) found that the tensile strength of hard sandstone linearly increases with the logarithm of displacement rate which supports our findings for joint-segments of shorter lengths. Our results suggest that the changes in displacement rates can cause

strain-weakening or strain-hardening of materials with non-persistent joint-segment of variable lengths. The laboratory-estimated results either undermine or overestimate the actual strength of rocks in the field, however, the potential of damage substantially enhanced at faster displacement rates when accumulation of strain energy is at peak and the strength of the material considerably reduced when a critical value (0.15) of joint persistent ratio was crossed.

4.2 Effect of joint-segment with variable lengths

Several attempts were undertaken to assess the influence of different aspects of pre-existing joint on material strength, but our knowledge is limited by a paucity on how the length of the non-persistent joint influences the strength of material while compressed at varying displacement rates. Lajtai (1971) performed several tests on cubic samples by introducing pre-existing cracks ranging from 0.5 to 2 inches in length and found that the variation in failure strengths was comparatively higher for cracks aligned perpendicular to compression direction than that of cracks positioned along the compression axis. We observed from series two and three experiments that at displacement rates >4.45 mm/min, the strength of the material substantially decreased with increasing length of the non-persistent joint-segment beyond a critical threshold window of persistent ratio (0.15–0.20), while the strength generally enhanced for very slow to medium rates (≤ 3 mm/min) (figure 10). Also, slow rate of displacement has limited influence on jointed samples since the differences in strength for intact to single- and double-jointed samples were comparatively low at very slow to slow displacement rates, while the differences were high for fast to

very fast rates, therefore, fast displacement rate considerably affects the strength of the material (table 1). However, slow rates can correspond to creep of bulk material along the cracked surface beyond a critical value of the persistent ratio (0.20 in our assessment). Overall, the strength of the material decreased in the order of intact samples, samples with single and double-jointed segment(s) and support the findings from earlier studies (Yang *et al.* 2009; Yang and Jing 2011).

4.3 Variation in the types of fracturing

Second series of tests produced diverse patterns of crack for varying lengths of the initially fabricated joint-segment at different displacement rates (figure 6). The initiation of cracking activity began in the form of primary tensile wing cracks at the tip of the pre-existing joint-segment(s) followed by secondary shear or tension cracks propagating towards the bounding faces of the sample along the direction of axial displacement. Similar modes and temporal sequence of cracks were reported in other materials such as sandstone (Petit and Barquins 1988), marble (Jiefan *et al.* 1990; Chen *et al.* 1995), gabbro (Wong *et al.* 2007), and plaster of Paris (Lajtai 1974), however, the effect of displacement rate and varying lengths of initial joint-segment were excluded in these studies. We observed that slow rate of displacement initiated stable and progressive growth of primary tensile wing cracks, while fast rate mostly developed shear fracture along the displacement direction when the persistent ratio was low. Samples with high persistent ratio initiated quasi-planar secondary shear cracks along the orientation of the initial joint-segment and caused early failure of samples. Additionally, the crack propagated at faster pace when the length of the pre-existing joint was maximum (25 mm) irrespective of the displacement rates caused premature failure. The samples were extensively damaged at fast displacement rate followed by spalling off near surface materials along the fractured surfaces.

The pattern of cracks was different for double-jointed samples in series-three experiments (figure 9) compared to the single jointed samples in series-two (figure 6). Different fracture geometries impose contrasting stress regimes in the crack bridge area (Shen *et al.* 1995), however, limited is known for identical fracture geometry but at varying loading situations. We found that at

medium to very fast-displacement rates, the crack coalescence mechanisms were dominant in the bridging area that was separated by the initial joint-segments. Wong and Chau (1998) reported three major modes of coalescence pattern, i.e., shear (S) mode, mixed shear/tensile (M) mode, and wing tensile (W) mode which again further subdivided into nine minor modes. We observed M-II mode and S-mode when the rates of displacement were medium (3 mm/min) and fast (4.45 mm/min), respectively (figure 9c–d). At slow and very slow rates, tensile wing cracks developed around the tips of the pre-existing joint located either in the upper or lower half of the sample without any evidence of coalescence in the bridging region. This confirms the fact that rate of displacement has contrasting influences on the mechanisms of crack coalescence.

Overall, primary tensile wing crack was dominant throughout the three series of experiments, however, the timing, location and displacement rates associated with the secondary shear crack revealed useful insights to understand the mechanisms of cracking as failure often initiated with shear movement (table 2). The failure modes observed at varying displacement rates (figures 5, 6 and 9) for three series of experiments were summarized in figure 11 following the different failure mode types reported by Basu *et al.* (2013). The frequency of shear-induced failure enhances with the increment of the length of the joint-segment. The intact samples were failed under tensile splitting mode with occasional development of multiple fractures (figures 5 and 11). The secondary shear appeared with a condition when the persistent ratios were low. Samples with lowest persistent ratio (0.10) allowed the growth of shear fracture when the displacement rate crossed a critical value (3 mm/min), while the samples with second-lowest persistent ratio (0.15) initiated shearing when the primary tensile wing crack reached an optimum length (figures 6 and 11). With the further enhancement of the persistent ratio (>0.15), the respective contribution of shearing mechanisms increased in addition to the primary tensile cracking as quasi-planar secondary shear fractures started to develop along the direction of fabricated joint-segment(s) (figures 6 and 11). It was observed that the shearing activities were abundant when the displacement rates were comparatively faster, however, slow rates initiated early occurrence shearing when the length of the single joint-segment was highest (25 mm). The second hypothesis

Table 2. Failure modes of the intact (series one), single (series two) and double (series three) cracked samples at different rates of displacement.

| Length of segment | Displacement rates (mm/min) | | | | |
|-------------------|-----------------------------|----------------|-----------------|----------------|--------------------|
| | 0.048 (very slow) | 0.12 (slow) | 3.0 (medium) | 4.45 (fast) | 6.0 (very fast) |
| Intact | AS | MF | AS | AS | MF |
| 10 mm | AS | AS | MF | MF | YSF |
| 15 mm | AS | SASP | AS | MF | AS |
| 20 mm | AS | YSF | DS | DS | SASP |
| 25 mm | YSF | YSF | DS | AS | SASP |
| Double | AS | AS | AS | SASP | AS |

Note: AS: Axial splitting, MF: Multiple fractures, YSF: Y-shaped fracture, SASP: Shearing along single plane, DS: Double shear.

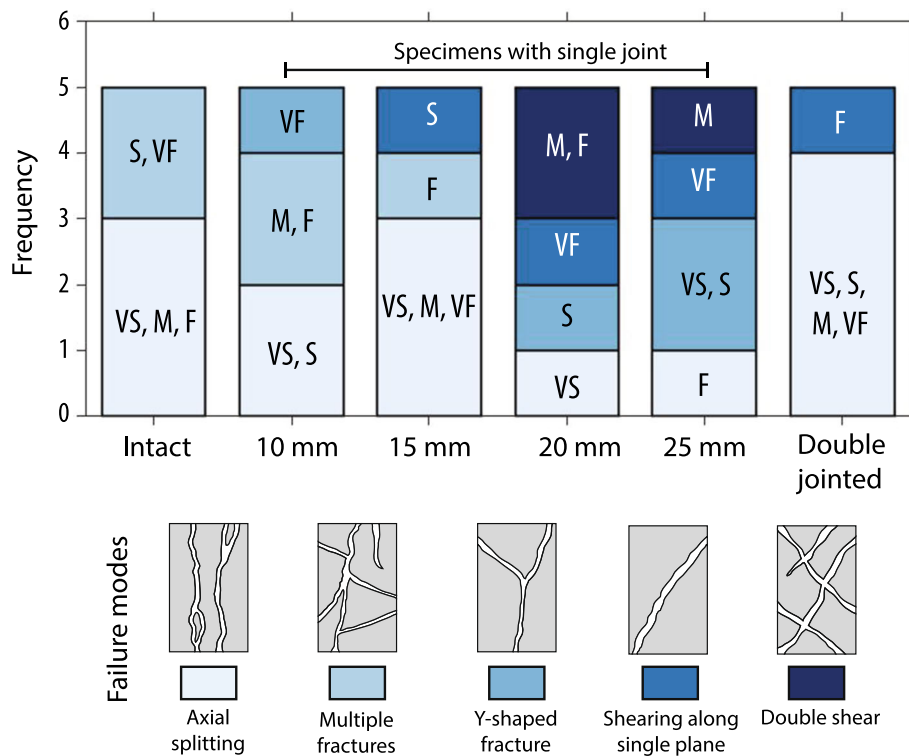


Figure 11. Bar diagram showing different failure modes for intact, single and double cracked specimens under compression at varying ranges of displacement rates. Schematic illustrations of different modes of failure are presented in the legend. The text in the bar plot represents varying rates of displacement (in mm/min) during the axial compression. The abbreviations used in the figure are as follows. VS: Very slow (0.048 mm/min), S: Slow (0.12 mm/min), M: Medium (3.0 mm/min), F: Fast (4.45 mm/min), VF: Very fast (6.0 mm/min). Schematic illustration of different failure modes is modified after Basu *et al.* (2013).

assessing the potential of developing secondary shearing activity at faster rates holds true and high persistent ratio of non-persistent joint-segment sometimes accelerates the mechanisms by forming shear cracks at early stages of cracking even at slow displacement rate.

The failure mechanisms associated with the coalescence of multiple non-persistent joint-segments have a significant effect on the stability of rock mass. Hence, geotechnical constructions

founded in rocks and are experiencing exogenic factors such as blasting, drilling, seismic and thermal forces require additional prevention strategies to avoid enhanced displacement rate-related instability.

4.4 Significance and implications of this study

The different outcomes of the experimental results discussed above have significant implications to

integrate the changes in strength of material with control parameters, i.e., joint persistent ratio and rate of displacement. The three vertices of the concept-triangle in figure 12 represent the boundary conditions of material response under varying displacement conditions as identified by Ožbolt *et al.* (2006). The inertial responses mostly depend on the strength of material such as rock exerts with more repulsive response than soils under external deformational forces. We have considered gypsum as an experimental material mostly because of its characteristics for reproducing molded cast of various shapes and forms, however, another important aspect is that it integrates both the properties of rocks and soils as shown in the diagram illustrating strength and inertial forces increase gradually from soil, gypsum to rock. The three series of experimental investigations confirmed that strength decreases in the order from intact to single-jointed with increasing length segment to double-jointed molded cast of gypsum samples of identical size and shape (figure 10). From the experimental results, we have found that enhancing the persistent ratio of joints leads to shearing of materials along the fractured surfaces

(samples with single-jointed segment of 20 and 25 mm length and double-jointed samples with overall 30 mm length segments), while lowering the ratio (single-jointed samples with 10 and 15 mm length segments) mostly enhances stress concentration at the induced crack tip favouring the development of tensile cracks.

The mechanisms of cracking at different modes because of joint-segment with variable persistent ratios under varying range of compressive forces were summarized in inserts (a–d) in figure 12. In addition to the tensile and shear-dominated regions, the research identified a zone of mixed response of tensile and shearing activities. The low persistent ratio of non-persistent joint-segment developed tensile wing cracks at the induced crack tip that further initiate tensile crack around the tip of the developing crack and finally propagated along the displacement direction (figure 12a). In contrast, the high persistent ratio mostly caused shearing of material along the induced cracked surfaces (figure 12c–d), while the region shaded in grey incorporates both the dynamics of tensile and shearing modes (figure 12b). Tensile mode of cracking developed initially followed by the

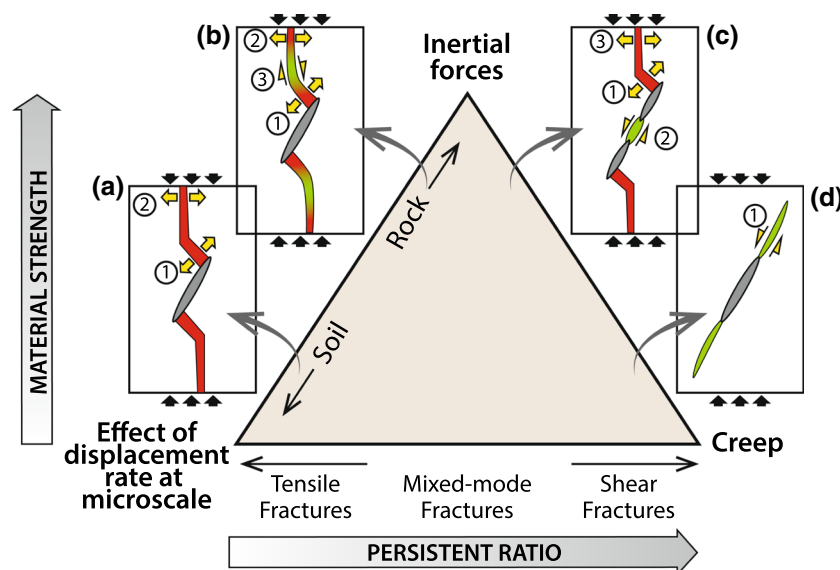


Figure 12. The outcomes of the experimental investigation summarized in the concept diagram in the form of a central triangle representing the consequences of different displacement rates and by integrating material strength and persistent ratio of non-persistent joint-segment(s). The three vertices of the deformation triangle outlined the boundary conditions in response to varying displacement rates. The strength of the material increases from soil to rock as the inertial forces enhanced accordingly in a similar order. Creep of the bulk material along the fractured surfaces implied shearing and the process further escalate when the persistent ratio of joint segments reached a critical value (0.20) or the displacement rate operates beyond a pedantic threshold (3 mm/min). The corresponding mechanisms of fracturing are shown in the insets (a–d). Grey ellipse(s) represents preexisting crack(s), and tension and shearing modes of cracking are shown by red and green colour, respectively. The sequence of development of cracks is displayed by the ascending numerical order. The modes of cracking dominated by primary tensile wing crack followed by the development of secondary shear crack and the possibility of developing early shearing mostly depends on the displacement rate and joint persistent ratio.

shearing mode in the region of mixed modes, however, the order of the cracking modes mostly depends on the persistent ratio of the induced or inherent fracture. Finally, it is evident from the three series of experimental investigations that progressive enhancement of joint persistent ratio sequentially develops cracks in the order of tensile to shearing mode. Also, high persistent ratio of joint-segment(s) witnessed enhancement in strength within slow rates of displacement while high rates correspond to decrease in strength (figure 10).

5. Conclusions

This study investigated the displacement rate dependency on the mechanical behaviour of pre-cracked samples made of gypsum, under unconfined axial compressive forces. Three series of experiments have been conducted: intact samples, samples with single joint-segment of variable lengths, and samples with two joint-segments of identical length separated by a bridge.

We show that different rates of displacement have diverse effects on the mechanical behaviour of molded gypsum with non-persistent joint. The strength of intact and samples with single joint-segment with low persistent ratios (0.10–0.15) experienced enhancement in strength with increasing displacement rates. Samples with high persistent ratios (0.20–0.30) show initial increase in strength at low rates followed by decrease in strength at high rates. A critical rate of displacement of 3 mm/min has been identified. The strength of material at varying displacement rates is significantly controlled by the persistence ratio of the intersecting joint(s) and progressively decreases from intact to single to double joint-segmented samples. The difference between maximum and minimum strengths decreased with the similar order. Also, the single joint-segment with short lengths manifested maximum change in strength than the joint-segment of larger lengths where the variations were limited.

In addition to the strength and deformational behavior, significant changes were observed in the mechanisms of fracturing and patterns of damage with the increasing displacement rates. The samples were extensively damaged when tested under faster displacement rates. Mainly two types of cracks developed from the pre-existing joint-segment: (a) primary tensile wing cracks at the tips

of the initial joint that gradually propagated towards the direction of maximum compression, and (b) secondary shear cracks that also initiated at the tips of pre-existing joint-segment(s) and propagated along either the direction of displacement or the coplanar direction of the induced joint-segment(s) and in some instances caused shear failure. Beyond a critical threshold (0.20) of persistent ratio of non-persistent joints, shear mode fracture development enhances at faster displacement rates (≥ 3 mm/min).

Acknowledgements

The authors thank Mr Rahul Kumar for his technical support in the Experimental Rock Deformation Laboratory of IIT Kanpur. GKM acknowledges a fellowship from IIT Kanpur for his MTech program. This work is a part of a Swarnajayanti Fellowship (DST/SJF/E&ASA-01/2015-16) and an Early Career Research Grant (ECR/2016/001988) awarded to SM. VM thanks a post-doctoral fellowship from the same Swarnajayanti Fellowship. The editor, associate editor and two anonymous reviewers are thanked for their valuable comments on the earlier version of the manuscript.

Author statement

Gaurav Kumar Mathur: Sample preparation and running experiments, data processing, writing original draft; Vikram Maji: Data processing, writing original and revised manuscripts; Santanu Misra: Problem development and conceptualization, supervision, funding, data processing, writing original and revised manuscripts; Gaurav Tiwari: Problem development and conceptualization, co-supervision, writing original manuscript.

References

- Alshkane Y M, Marshall A M and Stace L R 2017 Prediction of strength and deformability of an interlocked blocky rock mass using UDEC; *J. Rock Mech. Geotech. Eng.* **9(3)** 531–542, <https://doi.org/10.1016/j.jrmge.2017.01.002>.
- Atapour H and Moosavi M 2014 The influence of shearing velocity on shear behavior of artificial joints; *Rock Mech. Rock Eng.* **47(5)** 1745–1761, <https://doi.org/10.1007/s00603-013-0481-9>.
- Barton N 1973 Review of a new shear-strength criterion for rock joints; *Eng. Geol.* **7(4)** 287–332, [https://doi.org/10.1016/0013-7952\(73\)90013-6](https://doi.org/10.1016/0013-7952(73)90013-6).

- Barton N, Lien R and Lunde J 1974 Engineering classification of rock masses for the design of tunnel support; *Norg. Geotek. Inst. Publ.* **6**(106).
- Basu A, Mishra D A and Roychowdhury K 2013 Rock failure modes under uniaxial compression, Brazilian, and point load tests; *Bull. Eng. Geol. Environ.* **72** 457–475.
- Bobet A and Einstein H H 1998 Fracture coalescence in rock-type materials under uniaxial and biaxial compression; *Int. J. Rock Mech. Min. Sci.* **35**(7) 863–888, [https://doi.org/10.1016/S0148-9062\(98\)00005-9](https://doi.org/10.1016/S0148-9062(98)00005-9).
- Chen G, Kemeny J M and Harpalani S 1995 Fracture propagation and coalescence in marble plates with pre-cut notches under compression; In: *Proceedings of the Symposium on Fractured and Jointed Rock Masses* (eds Myer L R, Cook N G W, Goodman R E and Tsang C F, Lake Tahoe, CA, pp. 435–439.
- Dershowitz W S and Einstein H H 1988 Characterizing rock joint geometry with joint system models; *Rock Mech. Rock Eng.* **21** 21–51.
- Eshelby J D 1959 The elastic field outside an ellipsoidal inclusion; *Proc. Roy. Soc. A* **252**(1271), <https://doi.org/10.1098/rspa.1959.0173>.
- Ghazvinian A and Hadei M R 2012 Effect of discontinuity orientation and confinement on the strength of jointed anisotropic rocks; *Int. J. Rock Mech. Min. Sci.* **55** 117–124, <https://doi.org/10.1016/j.ijrmms.2012.06.008>.
- Gong F, Zhang L and Wang S 2019 Loading rate effect of rock material with the direct tensile and three Brazilian disc tests; *Adv. Civ. Eng.* **2019** 6260351, <https://doi.org/10.1155/2019/6260351>.
- Griffith A A 1921 The phenomena of rupture and flow in solids; *Phil Trans. Roy. Soc. A* **221** 582–593, <https://doi.org/10.1098/rsta.1921.0006>.
- Hoek E and Bray J D 1974 *Rock Slope Engineering*; 3rd edn, Taylor & Francis, CRC Press, 364p, <https://doi.org/10.1201/9781482267099>.
- Hoek E and Brown E 1997 Practical estimates of rock mass strength; *Int. J. Rock Mech. Min. Sci.* **34**(8) 1165–1186, <https://doi.org/10.7551/mitpress/7803.003.0005>.
- Horii H and Nemat-Nasser S 1986 Brittle failure in compression: Splitting faulting and brittle-ductile transition; *Philos. Trans. Roy. Soc. A* **319**(1549) 337–374, <https://doi.org/10.1098/rsta.1986.0101>.
- Ishii E 2016 Far-field stress dependency of the failure mode of damage-zone fractures in fault zones: Results from laboratory tests and field observations of siliceous mudstone; *J. Geophys. Res. Solid Earth* **121** 70–91, <https://doi.org/10.1002/2015JB012238>.
- Jafari M K, Pellet F, Boulon M and Hosseini K A 2004 Experimental study of mechanical behaviour of rock joints under cyclic loading; *Rock Mech. Rock Eng.* **37**(1) 3–23, <https://doi.org/10.1007/s00603-003-0001-4>.
- Janach W 1976 The role of bulking in brittle failure of rocks under rapid compression; *Int. J. Rock Mech. Min. Sci. Geomech. Abstr.* **13**(6) 177–186, [https://doi.org/10.1016/0148-9062\(76\)91284-5](https://doi.org/10.1016/0148-9062(76)91284-5).
- Jiefan H, Ganglin C, Yonghong Z and Ren W 1990 An experimental study of the strain field development prior to failure of a marble plate under compression; *Tectonophysics*. **175**(1–3) 269–284, [https://doi.org/10.1016/0040-1951\(90\)90142-U](https://doi.org/10.1016/0040-1951(90)90142-U).
- Kronenberg A K, Russell J E and Handin J 1990 Mechanical anisotropy of gneiss' failure criterion and textural sources of directional behavior; *J. Geophys. Res.* **95**(L) 613–634.
- Kulatilake P H S W, He W, Um J and Wang H 1997 A physical model study of jointed rock mass strength under uniaxial compressive loading; *Int. J. Rock Mech. Min. Sci. Geomech. Abstr.* **34**(3–4) 692–693, [https://doi.org/10.1016/S1365-1609\(97\)00123-8](https://doi.org/10.1016/S1365-1609(97)00123-8).
- Kumar A 1968 The effect of stress rate and temperature on the strength of basalt and granite; *Geophysics* **33**(3) 501–510, <https://doi.org/10.1190/1.1439947>.
- Lajtai E Z 1971 A theoretical and experimental evaluation of the Griffith theory of brittle fracture; *Tectonophysics*. **11**(2) 129–156, [https://doi.org/10.1016/0040-1951\(71\)90060-6](https://doi.org/10.1016/0040-1951(71)90060-6).
- Lajtai E Z 1974 Brittle fracture in compression; *Int. J. Frac.* **10**(4) 525–536, <https://doi.org/10.1007/BF00155255>.
- Lankford J 1981 Mechanisms responsible for strain-rate-dependent compressive strength in ceramic materials; *J. Am. Ceram. Soc.* **64**(2) 33–34, <https://doi.org/10.1111/j.1151-2916.1981.tb09570.x>.
- Mandal N, Misra S and Samanta S K 2004 Role of weak flaws in nucleation of shear zones: An experimental and theoretical study; *J. Struct. Geol.* **26** 1391–1400, <https://doi.org/10.1016/j.jsg.2004.01.001>.
- Mauldon M 1994 Intersection probabilities of impersistent joints; *Int. J. Rock Mech. Min. Sci. Geomech. Abstr.* **31**(2) 107–115, [https://doi.org/10.1016/0148-9062\(94\)92800-2](https://doi.org/10.1016/0148-9062(94)92800-2).
- Miller D U and Deere R P 1966 Engineering classification and index properties for intact rock; *AFWL-TR-65-116 Research and Technology Division Air Force Weapons Laboratory, New Mexico* **1** 65–116.
- Misra S 2011 Deformation localization at the tips of shear fractures: An analytical approach; *Tectonophysics*. **503**(1–2) 182–187, <https://doi.org/10.1016/j.tecto.2010.09.030>.
- Misra S and Mandal N 2007 Localization of plastic zones in rocks around rigid inclusions: Insights from experimental and theoretical models; *J. Geophys. Res. Solid Earth* **112** B09206, <https://doi.org/10.1029/2006JB004328>.
- Misra S, Ellis S and Mandal N 2015 Fault damage zones in mechanically layered rocks: The effects of planar anisotropy; *J. Geophys. Res. Solid Earth* **120**, <https://doi.org/10.1002/2014JB011780>.
- Misra S, Mandal N, Dhar R and Chakraborty C 2009 Mechanisms of deformation localization at the tips of shear fractures: Findings from analogue experiments and field evidence; *J. Geophys. Res. Solid Earth* **114** B04204, <https://doi.org/10.1029/2008JB005737>.
- Olsson W A 1991 The compressive strength of tuff as a function of strain rate from 10^{-6} to 10^3 /sec; *Int. J. Rock Mech. Min. Sci.* **28**(1) 115–118.
- Ozbolt J, Rah K and Meštrović D 2006 Influence of loading rate on concrete cone failure; *Int. J. Frac.* **139** 239–252, <https://doi.org/10.1007/s10704-006-0041-3>.
- Perkins R D, Green S J and Friedman M 1970 Uniaxial stress behavior of porphyritic tonalite at strain rates to 10^3 /second; *Int. J. Rock Mech. Min. Sci. Geomech. Abstr.* **7**(5) 527–535, [https://doi.org/10.1016/0148-9062\(70\)90005-7](https://doi.org/10.1016/0148-9062(70)90005-7).
- Petit J P and Barquins M 1988 Can natural faults propagate under Mode II conditions?; *Tectonics* **7**(6) 1243–1256, <https://doi.org/10.1029/TC007i006p01243>.
- Ramamurthy T and Arora V K 1994 Strength predictions for jointed rocks in confined and unconfined states; *Int. J. Rock*

- Mech. Min. Sci. Geomech. Abstr.* **31**(1) 9–22, [https://doi.org/10.1016/0148-9062\(94\)92311-6](https://doi.org/10.1016/0148-9062(94)92311-6).
- Rudnicki J W and Rice J R 1975 Condition for the localization of deformation in pressure-sensitive dilatant materials; *J. Mech. Phys. Solids* **23**(6) 371–394, [https://doi.org/10.1016/0022-5096\(75\)90001-0](https://doi.org/10.1016/0022-5096(75)90001-0).
- Sagong M and Bobet A 2002 Coalescence of multiple flaws in a rock-model material in uniaxial compression; *Int. J. Rock Mech. Min. Sci.* **39**(2) 229–241, [https://doi.org/10.1016/S1365-1609\(02\)00027-8](https://doi.org/10.1016/S1365-1609(02)00027-8).
- Shaunik D and Singh M 2019 Strength behaviour of a model rock intersected by non-persistent joint; *J. Rock Mech. Geotech. Eng.* **11**(6) 1243–1255, <https://doi.org/10.1016/j.jrmge.2019.01.004>.
- Shen B, Stephansson O, Einstein H H and Ghahreman B 1995 Coalescence of fractures under shear stresses in experiments; *J. Geophys. Res. Solid Earth* **100** 5975–5990, <https://doi.org/10.1029/95JB00040>.
- Sun S, Sun H, Wang Y, We J, Liu J and Kanungo D P 2014 Effect of the combination characteristics of rock structural plane on the stability of a rock-mass slope; *Bull. Eng. Geol. Environ.* **73**(4) 987–995, <https://doi.org/10.1007/s10064-014-0593-9>.
- Tiwari G and Latha G M 2019 Shear velocity-based uncertainty quantification for rock joint shear strength; *Bull. Eng. Geol. Environ.* **78**(8) 5937–5949, <https://doi.org/10.1007/s10064-019-01496-0>.
- Vazaios I, Vlachopoulos N and Diederichs M S 2018 Mechanical analysis and interpretation of excavation damage zone formation around deep tunnels within massive rock masses using hybrid finite–discrete element approach: Case of Atomic Energy of Canada Limited (AECL) Underground Research Laboratory (URL); *Can. Geotech. J.* **56**(1) 35–59, <https://doi.org/10.1139/cgj-2017-0578>.
- Wasantha P L, Ranjith P G, Xu T, Zhao J and Yan Y L 2014 A new parameter to describe the persistency of non-persistent joints; *Eng. Geol.* **181** 71–77, <https://doi.org/10.1016/j.enggeo.2014.08.003>.
- Wei S, Wang C, Yang Y and Wang M 2020 Physical and mechanical properties of gypsum-like rock materials; *Adv. Civ. Eng.* **17** 3703706, <https://doi.org/10.1155/2020/3703706>.
- Wong R H C and Chau K T 1998 Crack coalescence in a rock-like material containing two cracks; *Int. J. Rock Mech. Min. Sci.* **35**(2) 147–164, [https://doi.org/10.1016/S0148-9062\(97\)00303-3](https://doi.org/10.1016/S0148-9062(97)00303-3).
- Wong R H C, Guo Y, Chau K and Zhu W L S 2007 The crack growth mechanism from 3-D surface flaw with strain and acoustic emission measurement under axial compression; *Key Eng. Mater.* **4** 353–358, <https://doi.org/10.4028/www.scientific.net/KEM.353-358.2357>.
- Wyllie D and Mah C 2004 *Rock Slope Engineering*; 4th edn, CRC Press, <https://doi.org/10.1201/9781315274980>.
- Xu X Q, Liu B H, Wang Y, Li Y B and Xu J 2013 A numerical model on PVB laminated windshield subjected to headform low-speed impact; *J. Phys.: Conf. Ser.* **451**, <https://doi.org/10.1088/1742-6596/451/1/012016>.
- Yang S Q and Jing H W 2011 Strength failure and crack coalescence behavior of brittle sandstone samples containing a single fissure under uniaxial compression; *Int. J. Frac.* **168**(2) 227–250, <https://doi.org/10.1007/s10704-010-9576-4>.
- Yang S Q, Dai Y H, Han L J and Jin Z Q 2009 Experimental study on mechanical behavior of brittle marble samples containing different flaws under uniaxial compression; *Eng. Frac. Mech.* **76**(12) 1833–1845, <https://doi.org/10.1016/j.engfracmech.2009.04.005>.
- Zhao J 1997 Joint surface matching and shear strength. Part A: Joint matching coefficient (JMC); *Int. J. Rock Mech. Min. Sci. Geomech. Abstr.* **34**(2) 173–178, [https://doi.org/10.1016/S0148-9062\(96\)00062-9](https://doi.org/10.1016/S0148-9062(96)00062-9).

Corresponding editor: SAIBAL GUPTA